

Analysis of Hydrological and Suspended Sediment Events from Mad River Watershed using Multivariate Time Series Clustering

Ali Javed¹, Scott D. Hamshaw², Donna M. Rizzo², and Byung Suk Lee¹

¹Department of Computer Science, University of Vermont, Burlington, VT, USA

²Department of Civil & Environmental Engineering, University of Vermont, Burlington, VT, USA

Highlights

- This work is the first to apply a computational clustering approach to categorizing and analyzing hydrological storm events defined by multivariate time series.
- This work is the first to employ synthetically generated hydrological storm events (engineered to simulate real hydrological storm events) for model validation.
- This work is the first to study the relationship between 3-D time series clustering and 2-D hysteresis loop classification.

Abstract

Hydrological storm events are a primary driver for transporting water quality constituents such as turbidity, suspended sediments and nutrients. Analyzing the concentration (C) of these water quality constituents in response to increased streamflow discharge (Q), particularly when monitored at high temporal resolution during a hydrological event, helps to characterize the dynamics and flux of such constituents. A conventional approach to storm event analysis is to reduce the C-Q time series to two-dimensional (2-D) hysteresis loops and analyze these 2-D patterns. While effective and informative to some extent, this hysteresis loop approach has limitations because projecting the C-Q time series onto a 2-D plane obscures detail (e.g., temporal variation) associated with the C-Q relationships. In this paper, we address this issue using a *multivariate time series clustering* approach. Clustering is applied to sequences of river discharge and suspended sediment data (acquired through turbidity-based monitoring) from six watersheds located in the Lake Champlain Basin in the northeastern United States. While clusters of the hydrological storm events using the multivariate time series approach were found to be correlated to 2-D hysteresis loop classifications and watershed locations, the clusters differed from the 2-D hysteresis classifications. Additionally, using available meteorological data associated with storm events, we examine the characteristics of computational clusters of storm events in the study watersheds and identify the features driving the clustering approach.

Keywords: Hydrological storm event analysis, streamflow, suspended sediment, clustering, multivariate time series

1 Introduction

Characterizing the rainfall-runoff processes in watersheds is important for understanding the transport of water quality constituents through river systems, the sources of erosion (e.g., Sherriff et al., 2016), and our ability to evaluate model forecasts (Ehret and Zehe, 2011), all of which consequently help with the conservation and management efforts of watersheds (Bende-Michl et al., 2013). Examples of the latter include managing non-point source pollution (e.g., Chen et al., 2017) and monitoring for shifts in watershed function (e.g., Burt et al., 2015).

Watershed scientists and environmental managers analyze hydrological data (e.g., response of water quality constituents such as suspended sediment concentration) at the event scale — in this work, the

period of increased storm-runoff response above baseflow as a result of a rainfall event. Constituents are transported primarily during storm events and often show a high degree of variability, for example in the timing of sediment delivery relative to stream discharge, especially when observed with high frequency monitoring (Minaudo et al., 2017). Given the variability of both streamflow and water quality constituent responses during hydrological events, it is not surprising that the relationship between such water-quality constituents and discharge are similarly complex and typically cannot be described with simple linear relationships (Onderka et al., 2012). Despite the added complexity associated with this variation and highly dynamic behavior, the analysis of event concentration-discharge (C-Q) relationships has a long tradition in hydrology, geomorphology, and ecology to infer processes occurring within a watershed (Aguilera and Melack, 2018; Burns et al., 2019; Williams et al., 2018).

A fundamental feature of sediment and solute transport in rivers is that the concentration of such constituents are often not in phase with the associated stream discharge, resulting in hysteresis being present in the C-Q relationship. Williams (1989) is one of the first to use hysteresis patterns to study hydrological storm events, identifying six classes of hydrological events based on the shape of the hysteresis loops and offering linkages between the hysteresis classes and watershed processes. This hysteresis loop classification continues to be used in present time as a means to grouping storm events (e.g., Aguilera and Melack, 2018; Rose et al., 2018; Keesstra et al., 2019). The classification of hysteresis loops is usually done qualitatively using visual patterns (Hamshaw et al., 2018) or quantitatively using a hysteresis index (Lloyd et al., 2016b). While effective for inferring certain processes, this approach falls short in capturing the full *temporality* of variables, as it “collapses” their values as projected on the C-Q plane. The temporality may be seen in the rate of change (e.g., fast, slow), the orientation of change (e.g., clockwise, counter-clockwise), and the shape of change (e.g., linear, convex, concave) in the time series of the C-Q variables. With high frequency sensor data increasingly available, it is now possible to incorporate the temporality of variables into the analysis, towards further refining and adding to the existing hysteresis loop classification scheme. Additionally, hysteresis loop analysis typically does not consider the degree to which streamflow and suspended sediment return to base conditions at the end of an event - an important characteristic related to antecedent conditions and watershed characteristics.

A few hydrological studies have quantified the similarity between storm events defined by a single variable for categorization or other kinds of modeling (e.g., prediction). Ehret and Zehe (2011) propose a similarity measure to analyze discharge time series (a.k.a. “temporal sequence”) that uses feature extraction to leverage attributes of hydrographs such as the rising limb, peak and recession. Such manual feature extraction works well for hydrographs but may not generalize to other water quality time series. Ewen (2011) used a modified version of minimal variance matching (MVM) algorithm (Latecki et al., 2005) to quantify the similarity between storm events. Given a sequence of measurements in a hydrograph (called a “query sequence”), MVM finds a target hydrograph that contains a sub-sequence most similar to the query sequence. This similarity comparison, however, is not symmetric in both directions (i.e., $d(x, y) \neq d(y, x)$) as MVM can skip some elements of the target sequence (Latecki et al., 2005) and, therefore, is not appropriate for use in clustering. Wendi et al. (2019) use cross recurrence plots and recurrence quantification analysis to measure similarity between two hydrographs based on the recurring patterns. Recurrence quantification analysis quantifies the number and duration of recurrences of a dynamic system. Recurrence of subevents is not plausible for the work done at an event scale in this paper. None of these studies, however, was designed for storm events defined by multivariate time series.

In addition, a few other works have applied clustering on storm events defined by multiple variables. Bende-Michl et al. (2013) used high frequency data to build a database of variables such as precipitation, discharge, runoff coefficient, and maximum discharge, and then performed cluster analysis on these variables to understand nutrient dynamics in the Duck River. Minaudo et al. (2017) studied the relationship between phosphorous and discharge in hysteresis loops by generating high frequency estimates using non-linear

modeling (Jones et al., 2011). They used non-linear regression coefficients to cluster storm events. Mather and Johnson (2015) modeled event turbidity as a function of event discharge using a power-law based model. They used cluster analysis on the model parameters to select the number of hysteresis loop categories in developing their classification scheme, thereby avoiding the use of predetermined classes. None of these works, however, categorizes storm events by capturing the full temporality of variables as defined by the rate of change, the orientation of change and the shape of change in the time series of C-Q variables.

In this paper, we present a method to cluster multivariate water quality time series at the event scale. As an example, we use multivariate time series clustering on two variables: concentration (C) and discharge (Q) by modeling them as trajectories in a 3-D space defined by concentration, discharge, and time, i.e., C-Q-T plane. We use high-resolution riverine suspended-sediment concentration (SSC) time series – hereafter referred to simply as concentration – collected from six watershed sites in Vermont for up to three years and show proof-of-concept of applying the computational clustering methods to categorize hydrological storm events. The efficacy of the approach is demonstrated qualitatively using multi-dimensional event visuals and quantitatively using metrics that summarize event characteristics.

2 Study Area and Data

Our study area is located in the Mad River watershed in the Lake Champlain Basin and central Green Mountains of Vermont (see Figure 1). This area was selected primarily due to the availability of continuous streamflow and suspended sediment monitoring data (Hamshaw et al., 2018) and ongoing geomorphic and sediment dynamics studies at the University of Vermont (Stryker et al., 2017; Wemple et al., 2017). Data of more than 600 storm events were collected in this watershed (and its five sub-watersheds) from October 19th, 2012 to August 21th, 2016 (see Table 1). Hamshaw et al. (2018) previously used this dataset to automate the C-Q hysteresis loop classification and further refine the hysteresis classification of Williams (1989). Sensors were installed to gather discharge and turbidity data at 15 minute intervals at each of the five tributaries and the main stem shown in Figure 1. Suspended sediment concentration (SSC) was estimated from turbidity using regression relationships. Storm event identification from the continuous stream of data was done in a semi-automated fashion. Mad River watershed storm events also have associated meteorological data available as summarized in the 24 storm event metrics (see Table 2). Details on data collection and event pre-processing in the Mad River watershed can be found in Hamshaw et al. (2018).

The elevation of the Mad River watershed ranges from 132 m to 1,245 m above sea level, and is predominantly forested except for the valley bottom, which features agriculture, village centers, and other developed lands (see Table 3). The watershed has a mean annual precipitation ranging from approximately 1,100 mm along the valley floor to 1,500 mm along the upper watershed slopes (PRISM, 2019). Soils range from fine sandy loams derived from glacial till deposits in the uplands to silty loams derived from glacial lacustrine deposits in the lowlands. Erosional watershed processes include bank erosion, agricultural runoff, unpaved road erosion, urban storm water, and hillslope erosion. Similar to many watersheds in Vermont,

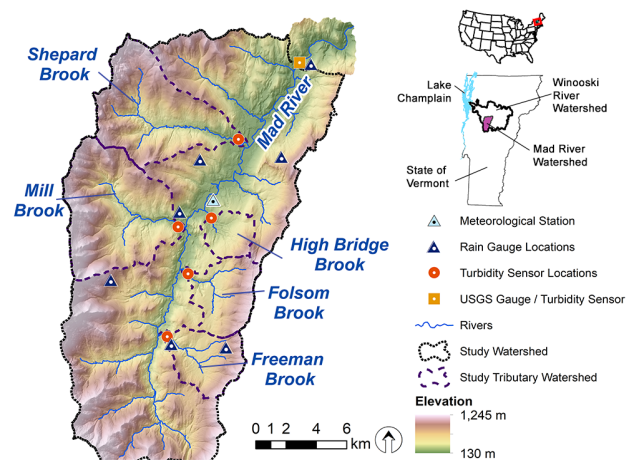


Figure 1: Study area locations within the Lake Champlain Basin of Vermont (Hamshaw et al., 2018).

Table 1: Number of storm events from each study watershed.

Site	Number of events monitored	Monitoring start date	Monitoring end date
Mad River (main stem)	148	Oct 29 th , 2012	Aug 21 th , 2016
Shepard Brook	106	Jul 18 th , 2013	Dec 23 rd , 2015
High Bridge Brook	41	Jun 6 th , 2013	Nov 17 th , 2013
Mill Brook	158	Oct 19 th , 2012	Dec 23 rd , 2015
Folsom Brook	96	Jul 17 th , 2013	Sept 13 th , 2015
Freeman Brook	54	Jun 2 nd , 2013	Nov 17 th , 2013
Total	603	Oct 19th, 2012	Aug 21th, 2016

Table 2: Description of the 24 storm event metrics used in this work.

Metric	Description
Hydrograph/ Sedigraph characteristics	
T_Q	Time to peak discharge (hr)
T_{SSC}	Time to peak TSS (hr)
T_{QSSC}	Time between peak SSC and peak flow (hr)
Q_{Recess}	Difference in discharge value at the beginning and end of event
SSC_{Recess}	Difference in concentration value at the beginning and end of event
HI	Hysteresis Index
Antecedent conditions	
T_{LASTP}	Time since last event (hr)
A3P	3-Day antecedent precipitation (mm)
A14P	14-Day antecedent precipitation (mm)
$SM_{SHALLOW}$	Antecedent soil moisture at 10 cm depth (%)
SM_{DEEP}	Antecedent soil moisture at 50 cm depth (%)
BF_{NORM}	Drainage area normalized pre-storm baseflow ($m^3/s/km^2$)
Rainfall characteristics	
P	Total event precipitation (mm)
P_{max}	Maximum rainfall intensity (mm)
D_P	Duration of precipitation (hr)
T_{PSSC}	Time between peak SSC and rainfall center of mass (hr)
Streamflow and sediment characteristics	
BL	Basin Lag
Q_{NORM}	Drainage area normalized stormflow ($m^3/s/km^2$)
$\text{Log}(Q_{NORM})$	Log-normal stormflow quantile (%)
D_Q	Duration of stormflow (hr)
FI	Flood intensity
SSC	Peak SSC (mg/L)
SSL_{NORM}	Drainage area normalized total sediment (kg/m^2)
$FLUX_{NORM}$	Drainage area and flow normalized sediment flux ($kg/m^3/km^2$)

reducing excessive erosion and sediment transport in the Mad River is a focus of the management efforts such as implementation of stormwater management practices, streambank stabilization, and river conservation.

Table 3: Key characteristics of the study watersheds.

Characteristic	Shepard Brook	High Bridge Brook	Mill Brook	Folsom Brook	Freeman Brook	Mad River
Area (km^2)	44.6	8.6	49.2	18.2	17.0	344.0
Minimum elevation (m)	195	225	216	229	266	140
Maximum elevation (m)	1117	796	1114	886	860	1245
Elevation range (m)	923	571	898	657	594	1105
Stream order	4th	3rd	4th	4th	4th	5th
Drainage density (km/km^2)	2.38	2.45	2.16	1.77	1.95	0.97
% Forested land	92.2	66.7	89.2	77.6	76.2	85.5
% Developed land	1.0	16.6	1.5	12.7	8.3	4.7
% Agricultural land	5.6	15.5	7.0	8.8	14.6	8.0
% Other land	1.1	2.1	0.8	0.7	1.7	1.1

3 Methods

3.1 Event time series processing

A time series is a sequence of variable values ordered by time and typically observed at a regular interval. In this work, sensor data collected for individual storm events are modeled as trajectories and are mathematically represented as multivariate time series. A *multivariate* time series is a times series of two or more variables combined. For example, two (univariate) time series, $T1 = \langle V1_1, V1_2, V1_3, \dots, V1_n \rangle$ and $T2 = \langle V2_1, V2_2, V2_3, \dots, V2_n \rangle$, when combined, make a bivariate time series $\mathbf{T} = \langle (V1_1, V2_1), (V1_2, V2_2), \dots, (V1_n, V2_n) \rangle$. (See Figure 2 for a matrix representation of a multivariate time series with m variables and n time steps.).

The environmental time series data in our work are collected in-situ by multiple sensors. These data typically contain noise and gaps, and therefore pre-processing (i.e., filtering and re-sampling) are often necessary. In addition, given that the data are delineated into hydrological events

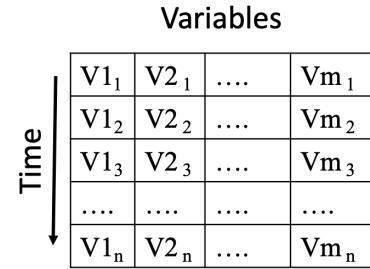


Figure 2: A matrix representation of multivariate time series (m variables, n time steps); a column for each variable and a row for variable value at each time step.

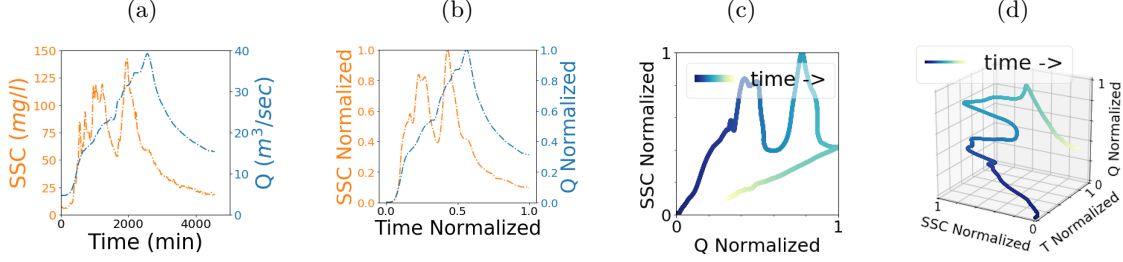


Figure 3: Pre-processing of storm events: (a) raw time series, (b) pre-processed time series, (c) C-Q plot, and (d) C-Q-T plot.

and our interest is in comparing the relationship between discharge and concentration, we normalized both of them within each event to facilitate the study of C-Q and C-Q-T plots (see Figure 3). Specifics of these pre-processing steps performed are as follows:

Smoothing. Discharge and concentration time series were smoothed to remove noise using the Savitsky-Golay Filter (Scipy, 2012). We selected a third-order, 21-step filter for the main stem of Mad River and a fourth-order, 13-step filter for the remaining sub-watersheds. Both choices of the filter order & step size were based on visual inspection of the resulting event time series to preserve the peaks and overall shapes, in the same manner as was done in the previous work by Hamshaw et al. (2018).

Re-sampling. Discharge and concentration time series were re-sampled to a uniform length of 50 samples using univariate spline fitting (Scipy, 2019). The length 50 was selected empirically as the minimum possible length that preserves the shape and characteristics of the event time-series. The re-sampling ensures that clustering is affected not by the length of the event but by the shape of the trajectory.

Normalization. Discharge and concentration time series were scaled to the range of 0 to 1 in their magnitude. This normalization ensures that the clustering is affected not by the magnitude of the individual times series but by the shape of the trajectory. (Normalization of magnitude is commonly used for a meaningful comparison of time series (Rakthanmanon et al., 2012).)

3.2 Concentration-discharge (C-Q) hysteresis classification

Each event in our dataset was categorized visually (by a human) in two classification schemes (see Figure 4): six classes of Williams (1989) and expanded 15 sub-classes of Hamshaw et al. (2018). We refer to categorization by Williams as “Classes” and the subcategories by Hamshaw as “Types” in this work. Class I and its subcategories represents C-Q relationships that show no hysteretic behavior. Class II represents those with clockwise hysteretic behavior and Class III with counter-clockwise, and their subcategories are differentiated by timing of the peak discharge and peak SSC influencing the shape of the hysteresis. A C-Q plot with a linear relationship followed by a clockwise loop is indicative of Class IV behavior; these patterns could reasonably be considered a special case of Class II (clockwise) hysteresis patterns, since they are linear first and then clockwise. The figure-eight shaped loops are represented as Class V, with subcategories discriminated by the loop orientation. Events that do not fall into any of the classes above were placed into the hysteresis class labeled “complex”.

3.3 Multivariate time series clustering

We clustered our multivariate time series data at the event scale into groups that correspond to various hydrograph and water quality (e.g., sedigraph) characteristics. To this end, significant effort was made to choose the clustering method. Paparrizos and Gravano (2016, 2017) conducted extensive benchmark tests on different clustering algorithms using multiple datasets from University of California at Riverside (UCR) time series repository (Dau et al., 2018) and found K-medoids with dynamic time warping (discussed in Section 3.3.2) to be the most accurate. Leveraging their work, we conducted additional benchmark tests

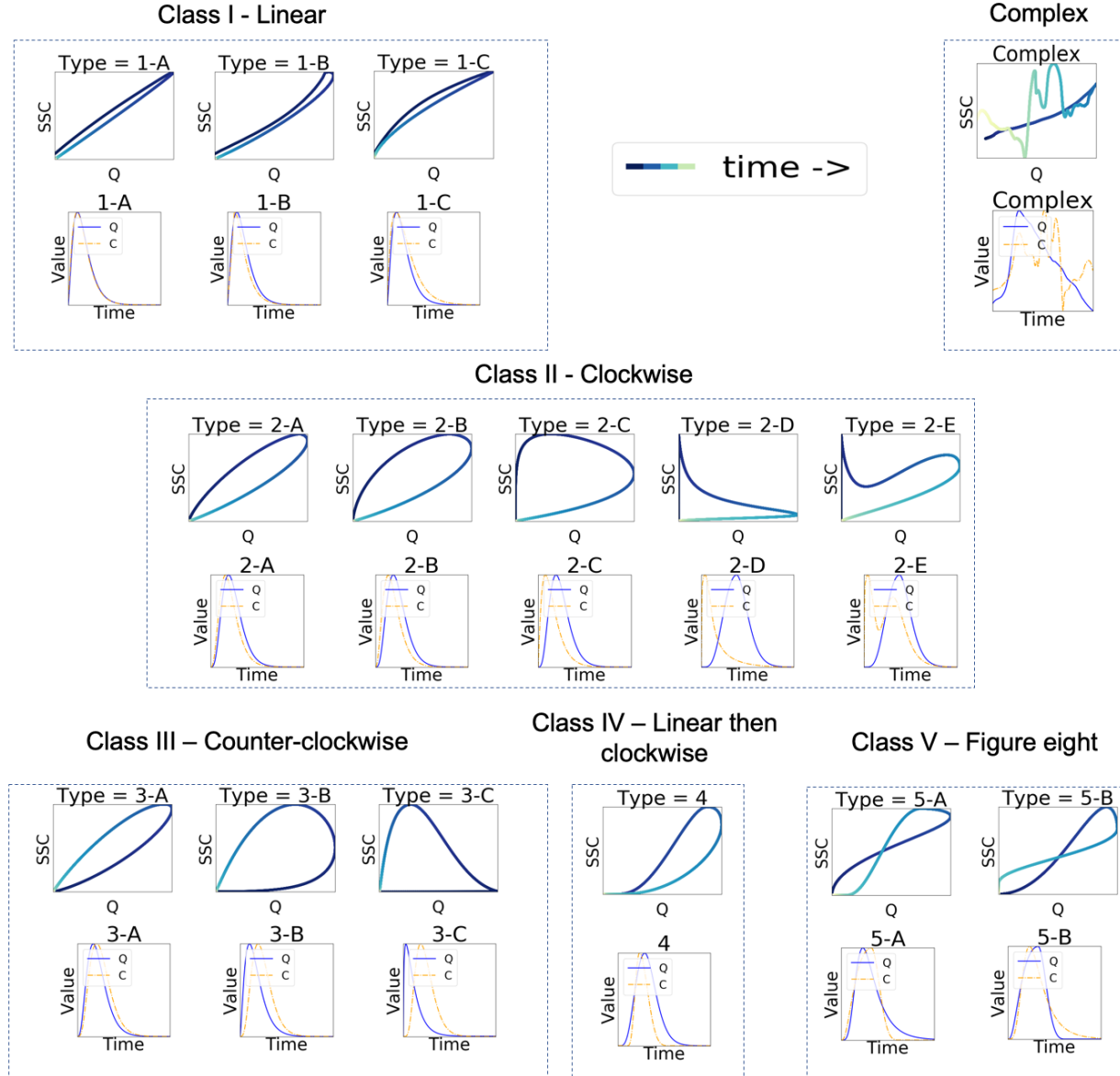


Figure 4: Classes of discharge-SSC hysteresis loops from events observed in the Mad River watershed. Solid line indicates hydrograph and dashed line indicates sedigraph.

on four different algorithms — TADPole (Begum et al., 2015), Kshape (Paparrizos and Gravano, 2016), K-medoids (Dynamic time warping), K-medoids (Euclidean) — using all 128 datasets currently present in the UCR time series repository (Dau et al., 2018) and found K-medoids with dynamic time warping to be most accurate (highest average Rand Index). All event times series data were pre-processed as outlined in Section 3.1.

3.3.1 K-medoids clustering algorithm

K-medoids is a variant of the popular K-means (Wu et al., 2007), where the cluster centroids are actual data points (called “medoids”) as opposed to coordinates as in K-means. These data points are in an n -dimensional space mapped from a multivariate time series of length n , where at each time step is a vector of the multiple variables (e.g., $V1, V2, \dots, Vm$ in Figure 2). Like K-means, K-medoids is an iterative algorithm (see Algorithm 1) where the initial centroids are randomly selected. The algorithm comprises two phases: the phase 1 assigns data points to clusters (Line 4 of Algorithm 1) and the phase 2 calculates new centroids for each cluster (Line 5 of Algorithm 1). In the first phase, the distance between all data points and each of the centroid is calculated, and each data point is assigned to the closest centroid. In the second phase, a new centroid is selected from each cluster by finding the data point that minimizes the sum of distances from it to all other data points in the cluster (called the “cost of configuration”). These two phases are repeated for a fixed number of times or until there is no change in the centroid selection. Algorithm 1 was implemented in Python (version 3.6.1); the source code can be found at Javed (2019b).

Algorithm K-medoids

Input: storm events (i.e., their multivariate time series representations); number k of clusters to be generated

Output: k clusters generated from the events

Procedure

// Initialize random seeds.

- 1 Randomly select k events as medoids from the input events.
- 2 **while** *termination criterion is not met* **do**
- 3 // Termination condition can be convergence of medoids or maximum allowed iterations.
- 4 Phase 1: Assign each event to its closest medoid.
- 5 Phase 2: From each cluster consisting of the medoid and events assigned to it, select an event that gives the smallest sum of distances to all the other events in the cluster and make the selected event a new medoid.
- 6 **end**
- 7 Return each cluster consisting of a medoid and all other events assigned to it.

Algorithm 1: K-medoids algorithm for storm event clustering.

3.3.2 Dynamic time warping

In order to cluster storm events represented by concentration and discharge time series, we used a variant of dynamic time warping (DTW) to calculate the “distance” between two multivariate times series representing different storm events. Originally introduced for speech recognition (Sakoe and Chiba, 1978), DTW is now arguably the most popular distance measure for time series data and is particularly appealing for data generated in the hydrological environment because of (i) the difficulty in defining the beginning and end of a hydrological event (i.e., the ambiguity inherent in event delineation), and (ii) the presence of noise in the sensor data (e.g., fouling).

Figure 5 illustrates how the distance is calculated between two time series (blue and red) using DTW compared to the more common Euclidean distance. While the Euclidean distance metric uses a one-to-one alignment; DTW employs a one-to-many alignment. This one-to-many alignment allows DTW to warp the time dimension so as to minimize the distance between the two time series. DTW can optimize alignment, both global alignment (by shifting the entire time series left or right) and local alignment (by stretching or squeezing sections of time series). This warping is often constrained to a limited neighborhood defined by a window. Experiments conducted by Paparrizos and Gravano (2016) showed the best accuracy (as measured by Rand Index) was obtained by constraining DTW to a limited window. Our intuition is that such a constraint results in better accuracy on average since too much flexibility may result in falsely high similarity values. Moreover, constraining the window size to 10% of the data is usually considered more than adequate for real-world applications (Ratanamahatana and Keogh, 2004). We also use this 10% window constraint in our calculation of DTW, because it allows flexibility in approximating the beginning and end of a hydrological event. DTW-D was implemented in Python (version 3.6.1); the source code can be found at Javed (2019a).

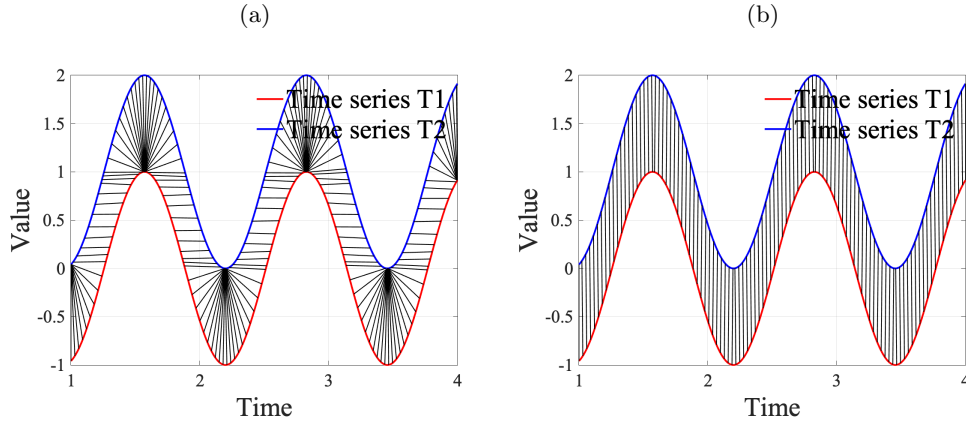


Figure 5: Illustration of the alignment between two times-series for calculating distance in (a) dynamic time warping (one-to-many) and (b) Euclidean (one-to-one).

Aligning two time series $T1$ of length a and $T2$ of length b using DTW involves creating a $a \times b$ matrix, D , where the element $D[i, j]$ is the square of Euclidean distance, $d(t1_i, t2_j)^2$, where $t1_i$ is the i th point of $T1$, $t2_j$ is the j th point of $T2$, and $d(\cdot, \cdot)$ is the Euclidean distance. A warping path P is a sequence of matrix elements that are mapped between $T1$ and $T2$ (Figure 6). This warping path must satisfy the following three conditions.

- Every point from $T1$ must be aligned with one or more points from $T2$, and vice versa.
- The first points of $T1$ and $T2$ must align, and so must their last points. In other words, the warping path must start and finish at diagonally opposite corner cells of the matrix.
- No cross-alignment is allowed, that is, the warping path must increase monotonically in the matrix plot.

Among all paths in the matrix that satisfy the three conditions above, we are interested in finding the path that minimizes the distance calculated as shown in Equation 1 (Shokoochi-Yekta and Keogh, 2015).

$$DTW(T1, T2) = \min_{P \text{ between } T1 \text{ and } T2} \sqrt{\sum_{(i,j) \in P} D[i, j]}, \quad (1)$$

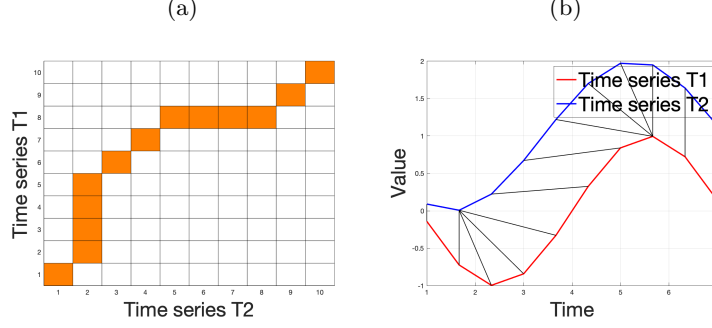


Figure 6: Illustration of finding an optimal alignment: (a) a matrix showing the warping path, i.e., an optimal alignment of time series $T1$ and $T2$ in DTW, where each cell (i, j) is the distance between i th element of $T1$ and j th element of $T2$ and the DTW distance is the sum of distances on the optimal path shown in orange, and (b) optimal alignment of each point in time series $T1$ (blue) and time series $T2$ (orange) is shown with black lines.

which enumerates over all possible warping paths P between $T1$ and $T2$ and finds the optimal warping path that minimizes the distance. Algorithm 2 outlines the steps to calculate $DTW(T1, T2)$.

Algorithm DTW

Input: $T1$ and $T2$: time series, W : warping window size

Output: distance between $T1$ and $T2$

Procedure

- 1 Let a and b be the lengths of $T1$ and $T2$, respectively.
- 2 Let m be the number of variables in $T1$ and $T2$ respectively.
- 3 Create a distance matrix D of size $a \times b$ and initialize all matrix elements to ∞ .
- 4 $D[0, 0] := 0$. // Initialize the first entry in D .
- 5 $i := 1$. $j := 1$. // Initialize the index of a warping path between $T1$ and $T2$.
- 6 **while** $i \leq a$ and $j \leq b$ **do**
 - 7 Calculate the squared Euclidean distance, $\sum_{c=1}^m (t1_{i,c} - t2_{j,c})^2$, between the i th item in $T1$ and each of the j th item in $T2$ within the range of $j = [i - W, i + W]$.
 - 8 Update $D[i, j]$ to $d(t1_i, t2_j)^2 + \min\{D[i - 1, j], D[i, j - 1], D[i - 1, j - 1]\}$.
 - 9 increase i by 1.
- 10 **end**
- 11 return $\sqrt{D[a, b]}$.

Algorithm 2: Dynamic time warping algorithm for distance calculation between two time series.

In this work, the sensor times series are multivariate (precisely, bivariate) defined by the discharge and SSC. We have considered two variants of DTW, DTW-independent (DTW-I) and DTW-dependent (DTW-D). DTW-I calculates the distance as the sum of distances that are calculated separately for individual variables (calling the DTW for each variable). DTW-D, on the other hand, handles $T1$ and $T2$ as multivariate time series and calls the DTW once. The dependency between discharge and concentration is important in our work and, therefore, we used DTW-D.

3.4 Experimental test cases

3.4.1 Synthetic hydrograph and sedigraph dataset

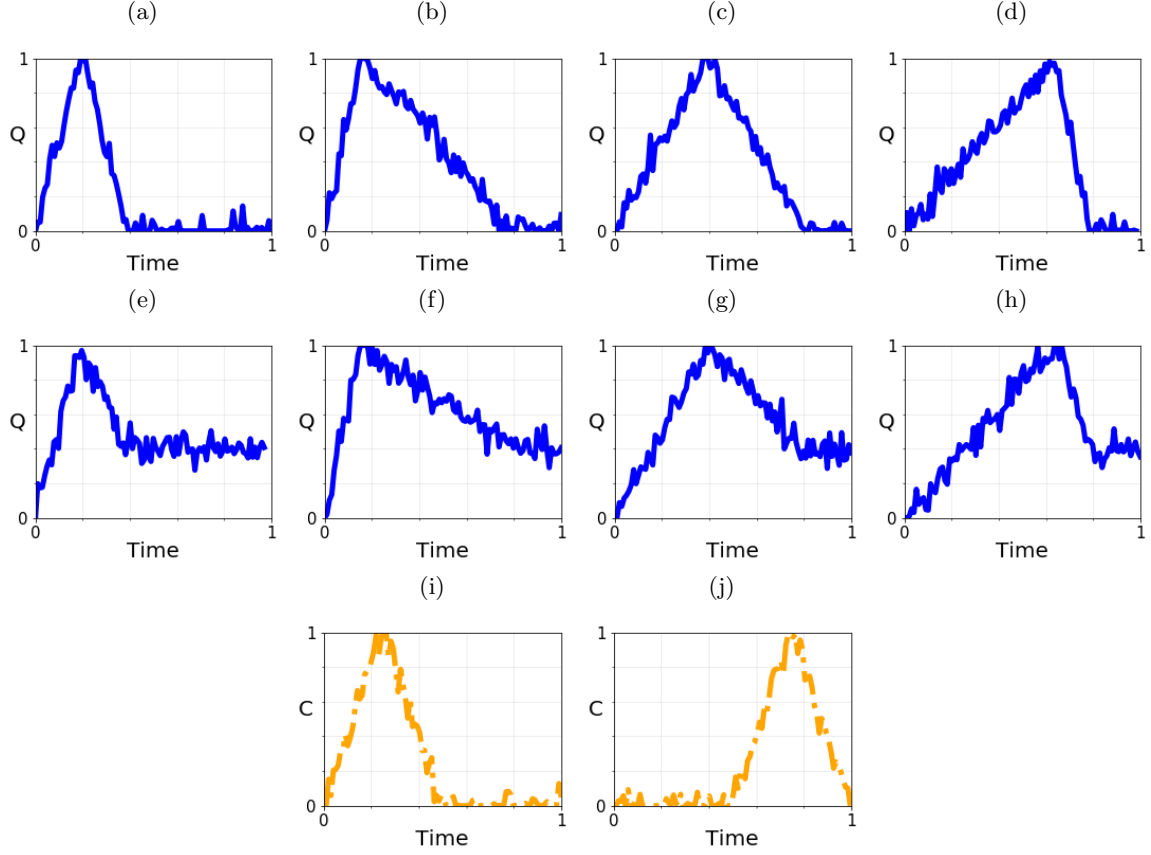


Figure 7: Eight types of synthetic hydrographs: (a) Flashy – very early peak – complete recess, (b) Early peak – complete recess, (c) Mid-peak – complete recess, (d) Delayed peak – complete recess, (e) Flashy – very early peak – incomplete recess, (f) Early peak – incomplete recess, (g) Mid-peak – incomplete recess, (h) Delayed peak – incomplete recess, and two different types of synthetic concentration graphs: (i) Early peak, (j) Late peak.

To help validate the computational clustering method, we generated synthetic (i.e., not obtained through measurement (Wikipedia, 2019)) hydrographs and sedigraphs using domain knowledge. These synthetic data can be labeled and used as the ground truth to facilitate the process of assessing methodology. A dataset generator was designed to produce synthetic hydrographs and concentration-graphs that contained realistic levels of sensor noise. Four control parameters were used: time-to-peak, duration-of-peak, onset, and recess. Time-to-peak controls the duration it takes for the concentration/discharge values to reach peak value of 1, duration-of-peak controls the duration of flow above base conditions, onset controls the “time” at which values (either concentration or discharge) start to rise in magnitude above base conditions, and recess controls the degree to which concentration/discharge values return to base conditions at the end of an event. Table 4 shows the values (between 0 and 1) for each of these parameters for the different types of synthetic graphs generated.

Examples of eight types of synthetic hydrographs and two types of synthetic concentration-graphs (see

Table 4: Default parameter settings for synthetic hydrograph and sedigraph generator.

Hydrograph				
Type	Duration-of-peak	Time-to-peak	Onset	Recess
Flashy - very early peak - Complete Recess	0.4	0.5	0	0
Flashy - very early peak - Incomplete Recess	0.4	0.5	0	0.4
Early peak - Complete Recess	0.8	0.2	0	0
Early peak - Incomplete Recess	0.8	0.2	0	0.4
Mid-peak - Complete Recess	0.8	0.5	0	0
Mid-peak - Incomplete Recess	0.8	0.5	0	0.4
Delayed peak - Complete Recess	0.8	0.8	0	0
Delayed peak - Incomplete Recess	0.8	0.8	0	0.4
Concentration-graph				
Type	Duration	Time-to-peak	Onset	Recess
Early peak	0.5	0.5	0	0
Late peak	0.5	0.5	0.5	0

Figure 7) shows different timings for the rise and fall of discharge and the concentration, respectively. Thus, when combining the eight types of hydrographs and the two types of concentration-graphs, the synthetic data represent sixteen possible types of storm events (see Figure 8). Random samples from a normal (Gaussian) distribution with a mean of 0.00 and standard deviation of 0.05 were added to the discharge and concentration value at each time step. We generated 800 synthetic storm events this way, equally distributed among the sixteen types.

3.4.2 Application to real hydrograph and sedigraph dataset

We applied the event clustering method to the Mad River watershed data. The time series of discharge and SSC were pre-processed (see Section 3.1), and used as input to K-medoids with the DTW-D algorithm. The resulting clusters of events were examined with respect to the following: (i) optimal number clusters, (ii) relationship to hysteresis loop (iii) relationship to watershed sites, (iv) discrimination of event characteristics through clustering and hysteresis, and (v) characteristic of event clusters (based on storm event metrics).

3.4.3 Finding the optimal number of clusters on the real data

In this work, we identified the “optimal” number of clusters for classification using the elbow method, in which the sum of squared errors (SSEs) are plotted against an increasing number of K clusters. A value for K is selected (visually) as the point where further increases in K result in diminishing reduction in SSE, thus making the onset of the plateau look like an elbow of an arm. In this respect, optimal K values were selected empirically, and then further validated using the Kneedle algorithm (Satopaa et al., 2011)).

3.5 Evaluation criteria

3.5.1 Clustering measures

We used three external measures of clustering to evaluate K-medoids with DTW-D on the synthetic storm event dataset — (a) Rand Index (b) Homogeneity and (c) Completeness. *Rand Index* is perhaps the most commonly used similarity measure between two different partitionings of a dataset, and is defined as the ratio of correct decisions over all decisions made, where a decision is made for each pair of elements in regard

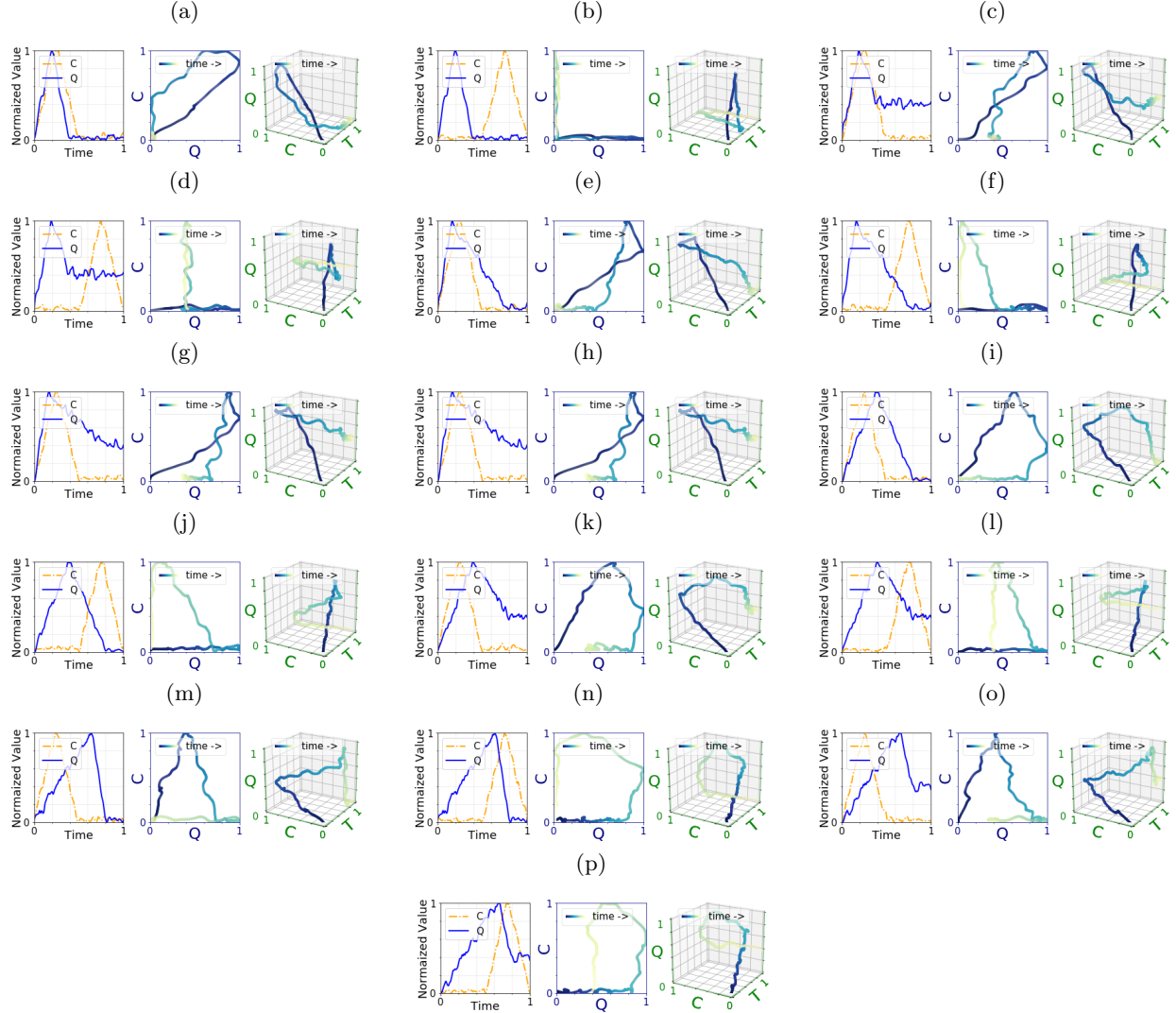


Figure 8: An example event from each class in the synthetic dataset: (a) Class 1, (b) Class 2, (c) Class 3, (d) Class 4, (e) Class 5, (f) Class 6, (g) Class 7, (h) Class 8, (i) Class 9, (j) Class 10, (k) Class 11, (l) Class 12, (m) Class 13, (n) Class 14, (o) Class 15, and (p) Class 16.

to putting both elements of the pair in the same cluster or different clusters. Its value ranges 0.0 to 1.0, where 1.0 means that the groups are identical and 0.0 means that the two partitionings do not agree on any pair of elements. *Homogeneity* ranges from 0.0 to 1.0, where 1.0 means that every cluster contains only elements that are members of the same class (see Figure 9a) and 0.0 means that there is only one cluster and every element in it belongs to a different class (see Figure 9b) (Rosenberg and Hirschberg, 2007).

Completeness ranges from 0.0 to 1.0, where 1.0 means that all elements of any given class are in the same cluster (see Figure 9c) and 0.0 means that there is only one class and every element in it is assigned to a different cluster (see Figure 9d) (Rosenberg and Hirschberg, 2007).

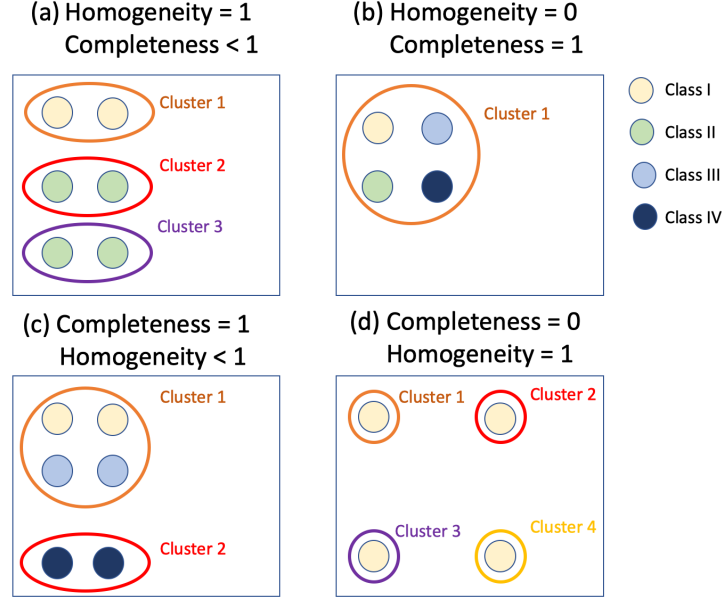


Figure 9: Schematic illustration of the measures – completeness and homogeneity with class representing ground-truth classifications.

3.5.2 Statistical measures

We used four statistical measures to study clustering performance – (a) Chi-squared test of independence, (b) One-way analysis of variance (ANOVA), (c) Z-score, and (d) Hopkins test. To investigate the dependency between computational clusters and watershed sites/hysteresis loop categories we used a Chi-squared test of independence. This test is used to determine if there is a significant relationship between two categorical variables. The null hypothesis for the test is that there is no relationship between the variables. We performed ANOVA test to investigate how well the 24 storm event metrics (see Section 2) for the storm events are explained by the Williams’s hysteresis loop classes and the computational clusters, respectively. ANOVA tests the null hypothesis that all groups have the same population mean. It does so by calculating the f-value as the ratio of the variance among group means over the average variance within groups to determine the ratio of explained variance to unexplained variance. For our purpose of clustering, a larger f-value indicates more accurate clustering, i.e., with higher inter-group similarity and lower intra-group similarity. To analyze the characteristics of each cluster using the 24 storm event metrics we used z-score value of each metric for each cluster. *Z-score* measures the number of standard-deviations the value of a metric is different from the mean metric value of all storm events. We compared the average metric value of events within a cluster to the average metric value of all events in the dataset. To measure the cluster tendency of a data set, we used Hopkins Test (Banerjee and Dave, 2004). *Hopkins test* tests the null hypothesis that data are generated by a Poisson point process and thus are uniformly randomly distributed. A value close to 1 indicates the data is highly clusterable, while a value close 0 indicates the data uniformly distributed.

4 Results

4.1 Validation of method using the synthetic dataset

Clusters resulting from K-medoids with DTW-D were identical to the ground truth (see Section 3.4). That is, K-medoids with DTW-D showed the score of 1.0 for all Rand Index, homogeneity and completeness despite the noise inherent in the synthetic dataset. Additionally, the synthetic dataset had a Hopkins test statistic of 1.00 indicating its high clusterability and suitability for use in clustering methods. Further, the elbow plot (see Figure 10) showed the elbow to be $k = 16$, after which the reduction in SSE was negligible. These results thus confirmed the validity of the method used.

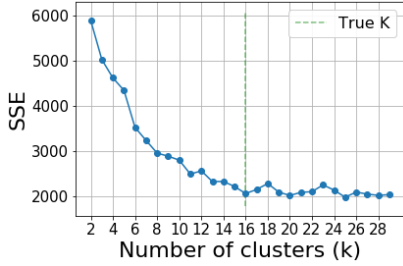


Figure 10: Sum of square error (SSE) for different number of clusters from the synthetic storm event dataset. (True value of $k=16$.)

Note that K-medoids with DTW-D was chosen not only for its high accuracy but also for the following advantages over each of the three other selected algorithms (see Section 3.3). TADPole requires an additional input parameter that is not very intuitive, in addition to the number of clusters (i.e., K). K-shape is inherently a univariate time series clustering algorithm and not applicable to multivariate time series. K-medoids with Euclidean distance does not have the flexibility of time series warping present in K-medoids with DTW-D, a quality we need in our algorithm given the approximate nature of event segmentation.

4.2 Application to real hydrograph and sedigraph dataset

4.2.1 Optimal number of clusters

The Mad River dataset had a Hopkins test statistic of 0.96, which indicates that the dataset is highly clusterable and, therefore, suitable to be used in clustering methods. Application of the K-medoids with DTW-D to the dataset ($N = 603$ storm events) yielded $k = 4$ clusters using both the elbow technique (Figure 11) and the Kneedle algorithm (Satopaa et al., 2011) (Section 3.4.3). The sizes of clusters were approximately 120 for three of them and 234 for one of them. Cluster 1 events tended to have broad clockwise hysteresis patterns with an early, and relatively short peak duration for SSC; the hydrograph raised quickly and nearly fully returned to baseflow (see Figure 12a). Cluster 2 events tended to have broader (less flashy) sedigraphs and hydrographs with streamflow not returning completely to baseflow levels (see Figure 12b). Cluster 3 events were similar to cluster 2, but had flashier and often multi-peaked sedigraphs that were shorter in duration (see Figure 12c). The timing of the peak of the sedigraph and hydrographs of cluster 4 events were typically delayed and tended to have an initial period of slow rise of sedigraph and hydrograph prior to the period of rapid rise (see Figure 12d). Events in cluster 4 tended to have hydrographs that return to near baseflow levels in contrast to cluster 2 and 3 events.

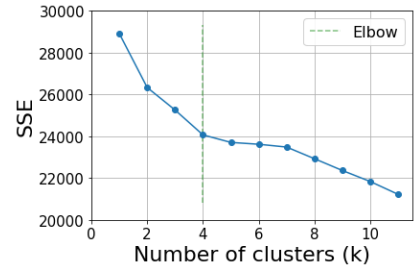


Figure 11: Sum of square error (SSE) for different number of clusters from the Mad River storm event dataset. (The elbow is at $k=4$.)

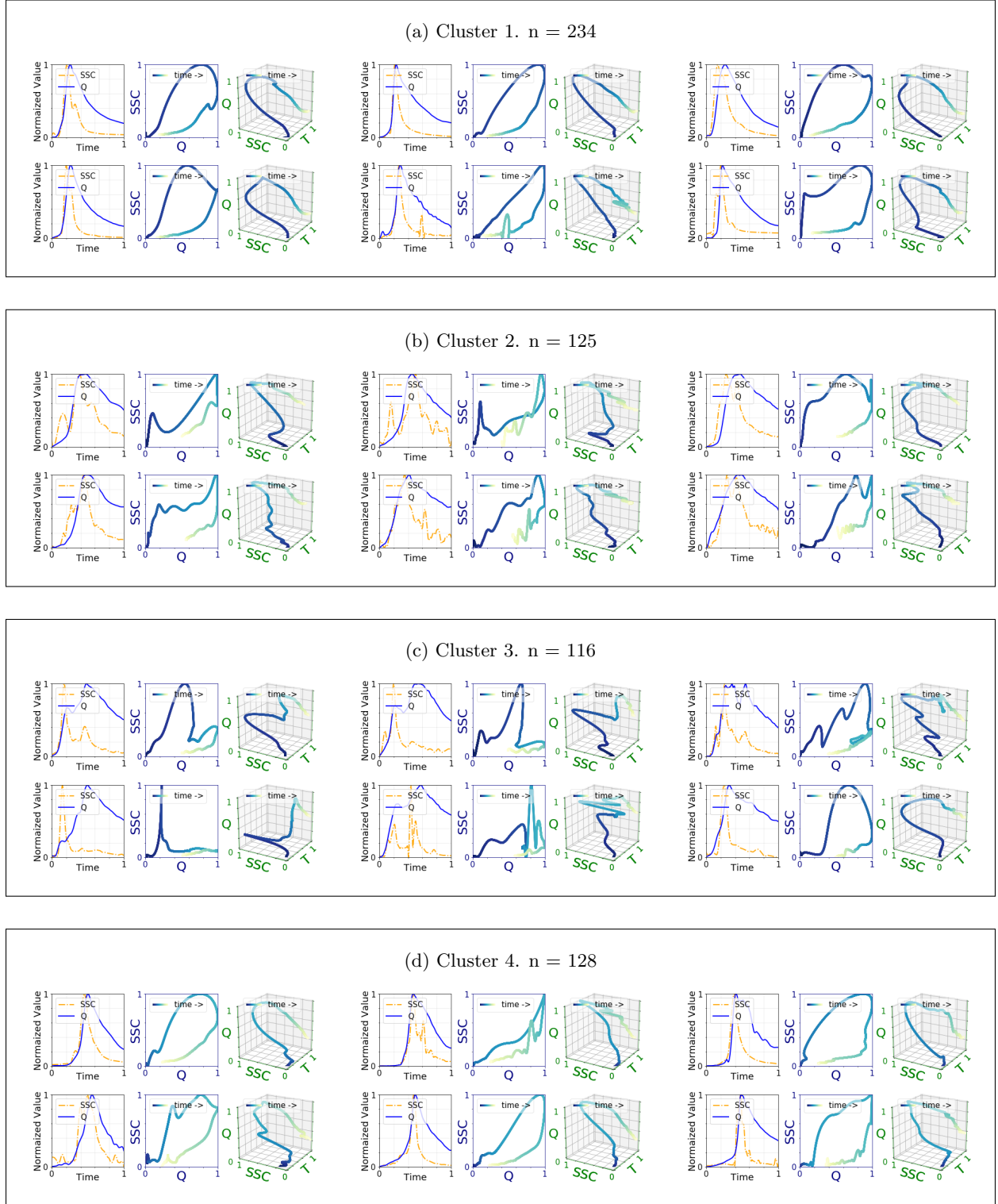


Figure 12: Six storm events closest to the centroid in each cluster of Mad River dataset ($k = 4$, $N = 603$).



Figure 13: Distribution of Williams' six classes in each cluster.

4.2.2 Relationship to hysteresis loops

Event cluster assignments did not correspond directly to the C-Q hysteresis classifications (see Section 3.2). The Mad River watershed events are severely skewed in the distribution of their hysteresis patterns when classified using Williams' classes (Table 5). That is, 63.8% of the 603 events belong to Class II and each of the remaining five classes contains only 5–10% of the events. In contrast, our computational clusters were relatively better balanced, with the largest of the four clusters containing only 39% events and all of the remaining clusters containing more than 18% of all events. Given the similarity of all the Mad River watershed sites (i.e., predominantly forested, mountainous watersheds), we would expect hydrological events to show a degree of similarity. This expectation was confirmed in the preponderance of Class II (clockwise) hysteresis patterns in the data. However, we found that our clustering did not classify events skewed to a single cluster, which would be expected given that our clustering method emphasizes the temporal aspect of the hydrograph and sedigraph more than the hysteretic aspect.

On the other hand, statistical test revealed that hysteresis classes and computational clusters were not independent of each other, hence correlated. Specifically, Chi-squared test of independence between hysteresis loop classes (both Williams' classes and Hamshaw's types) and computational clusters had a p-value lower than 0.001, thus establishing that they are not independent. For instance, (i) 43% of events in Class II appeared in the cluster 1 compared with no more than 21% in each of the other clusters, and (ii) only one (out of 30) event in Class I appeared in the cluster 3 (see Figure 13). A nontrivial portion of the Class II events and the Class IV events in the cluster 3, comprising 69% and 15%, respectively, of the events in that cluster, had the hysteresis loop pattern of linear-then-clockwise and overlapped between the two classes. In terms of Hamshaw's types, cluster 1 was dominated by Type 2-B (broad clockwise pattern) and cluster 3 was dominated by Type 2-D and Type 4 (narrow linear-then-clockwise pattern). The overlap between Class II and Class IV hysteresis classes is generally accepted in the study of hysteresis loops for watershed, and we also made the same observation from the storm events that belonged to the cluster 3 (see Figure 12).

Table 5: Distribution by hysteresis loop — Williams’ six classes(upper) and Hamshaw’s fifteen types (lower).

Cluster	Class I			Class II					Class III			Class IV	Class V		Complex	Total
	1-A	1-B	1-C	2-A	2-B	2-C	2-E	2-D	3-A	3-B	3-C	4	5-A	5-B		
1	11			167					16			12	20		8	234
	6	4	1	13	64	42	33	15	4	2	10		17	3		
2	12			58					16			15	15		9	125
	4	5	3	12	20	9	13	4	4	10	2		10	5		
3	1			80					6			18	2		9	116
	0	1	0	0	11	18	11	40	1	3	2		2	0		
4	6			80					13			14	10		5	128
	2	3	1	12	29	11	13	15	2	5	6		8	2		
Total	30			385					51			59	47		31	603
	12	13	5	37	114	80	70	74	11	20	20		37	10		

Table 6: Distribution of Mad River watersheds storm events over clusters.

Cluster	Mad River	Shepard Brook	High Bridge Brook	Mill Brook	Folsom Brook	Freeman Brook	Total
1	44	45	18	68	34	25	234
2	62	18	3	18	12	12	125
3	15	23	14	35	20	9	116
4	27	20	6	37	30	8	128
Total	148	106	41	158	96	54	603

4.2.3 Relationship to watershed sites

Both the physical features of a catchment and characteristics of individual storm events have influence on the type of streamflow and SSC events that occur at a particular monitored site. Figure 14 shows the number and percentage of storm events in each cluster from all watersheds in the Mad River dataset. Chi-squared test of independence between watershed sites and clusters had a p-value less than 0.001, thus strongly indicating a correlation between the two. For instance, 42% of events from the main stem of Mad River watershed site were grouped in the cluster 2 (Figure 14). Moreover, the numbers of storm events from different watersheds in the cluster 2 were in the same order as the stream order of the watersheds and, related, the site 3, the smallest, had the smallest number (only three out of 41) of storm events that appeared in the cluster 2. This observation hints some correlation between the clusters and watershed size.

The correlation between watersheds and clusters makes sense given that we could expect a particular site to have a characteristic hydrograph and sedigraph to a certain extent. This can be inferred intuitively when we visually examine the storm evens in the cluster 2, for instance. Cluster 2 contained events with a low degree of discharge recession (i.e., high difference between discharge rates at the start and end, respectively, of the event) as well as low SSC recession. This makes sense given that watersheds with larger catchment areas — main stem of Mad River watershed has the largest catchment area in our study are — are likely to take longer to return to the base discharge and concentration quantities and may not completely do so before another event occurs.

4.2.4 Discrimination of event characteristics through clustering and hysteresis

Computational clusters differentiated storm events based on a set of storm event metrics that is different from the set of metrics by which storm events in Williams’ hysteresis loop classes were differentiated (see Table 7). Specifically, for 19 of the 24 storm event metrics, an ANOVA test showed that at least one of the clusters had a mean metric value that was significantly different (i.e., p-value < 0.05) from the mean

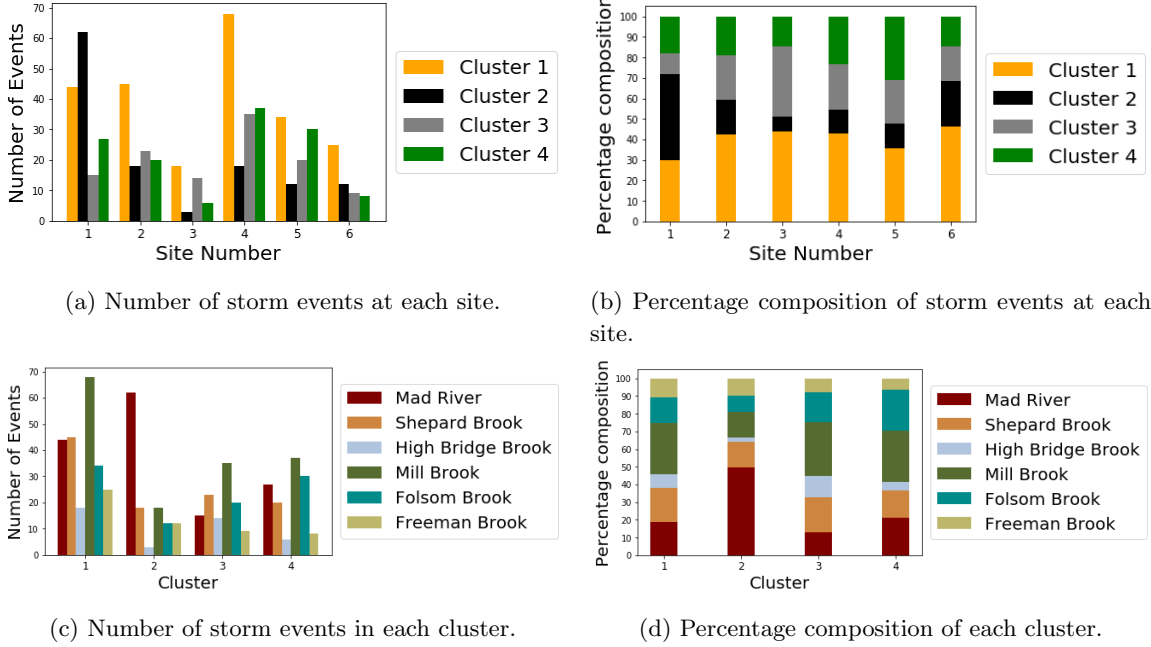


Figure 14: Cluster distribution over sites. The distribution of events in clusters is not in-dependant of sites with a p-value of less than 0.001 using a Chi-squared test of independence.

metric value of rest of the clusters, whereas for 11 metrics, one of the Williams' classes had a mean metric value that was significantly different from the mean metric value of the other Williams' classes. This is not surprising since both methods capture different features of the hydrograph and the sedigraph.

The hysteresis loop classes are designed to extract differences in the timing of the hydrographs and sedigraphs. This difference is the key to reflecting/preserving the shape of the hysteresis loops, and high emphasis is placed on the direction of the loop. Thus, it is not surprising that ANOVA test showed three of the metrics of Table 7 — HI (hysteresis index), T_{PSSC} (time between peak SSC and rainfall center of mass), and T_{QSSC} (time between peak SSC and peak flow) — to have the most explanatory power (as indicated by f-values) for hysteresis loop classes. This would be expected since these three metrics are directly indicative of the timing of SSC in relation to Q, which is key in determining the shape of a hysteresis loop.

In comparison, the explanatory power of clusters for distinguishing characteristics of events was based on a larger and more varied set of metrics (see Table 7). In contrast to the hysteresis classification, event clusters had significant differences across metrics associated with hydrograph and sedigraph characteristics — for instance, the timing of the peak of the hydrograph (T_Q) and sedigraph (T_{SSC}) as well as the difference between discharge/concentration values at the start of the event and end of the event (Q_{Recess} and SSC_{Recess}). This indicates that the clustering of events is driven by the hydrograph and sedigraph themselves as well as the relationship between the two.

Table 7: ANOVA test result using watershed performance metrics. F-value is shown in bold when the corresponding p-value is significant (i.e., < 0.05) and additionally marked with “**” if p-value < 0.0001 , and with “*” if p-value < 0.001 .

Metric	Description	F-value	
		Hysteresis loop	Time series clusters
Hydrograph/ Sedigraph characteristics			
T_Q	Time to peak discharge (hr)	0.78	50.82**
T_{SSC}	Time to peak TSS (hr)	1.10	39.69**
T_{QSSC}	Time between peak SSC and peak flow (hr)	45.96**	14.02**
Q_{Recess}	Difference in discharge value between the beginning and end of event	7.12**	91.64**
SSC_{Recess}	Difference in concentration value between the beginning and end of event	19.14**	20.30**
HI	Hysteresis Index	283.60**	12.21**
Antecedent conditions			
T_{LASTP}	Time since last event (hr)	0.46	1.92
A3P	3-Day antecedent precipitation (mm)	5.61*	12.82**
A14P	14-Day antecedent precipitation (mm)	2.92	7.26*
$SM_{SHALLOW}$	Antecedent soil moisture at 10 cm depth (%)	0.94	2.08
SM_{DEEP}	Antecedent soil moisture at 50 cm depth (%)	0.74	1.19
BF_{NORM}	Drainage area normalized pre-storm baseflow ($m^3/s/km^2$)	0.36	5.46
Rainfall characteristics			
P	Total event precipitation (mm)	4.01	10.72**
P_{max}	Maximum rainfall intensity (mm)	2.48	20.81**
D_P	Duration of precipitation (hr)	1.68	11.36**
T_{PSSC}	Time between peak SSC and rainfall center of mass (hr)	60.34**	22.69**
Streamflow and sediment characteristics			
BL	Basin Lag	6.03*	21.08**
Q_{NORM}	Drainage area normalized stormflow ($m^3/s/km^2$)	1.30	5.60*
$\text{Log}(Q_{NORM})$	Log-normal stormflow quantile (%)	4.95	25.10**
D_Q	Duration of stormflow (hr)	0.43	9.50**
FI	Flood intensity	2.25	8.90**
SSC	Peak SSC (mg/L)	0.74	8.63**
SSL_{NORM}	Drainage area normalized total sediment (kg/m^2)	2.50	1.76
$FLUX_{NORM}$	Drainage area and flow normalized sediment flux ($kg/m^3/km^2$)	10.52**	0.18

4.2.5 Characteristics of event clusters

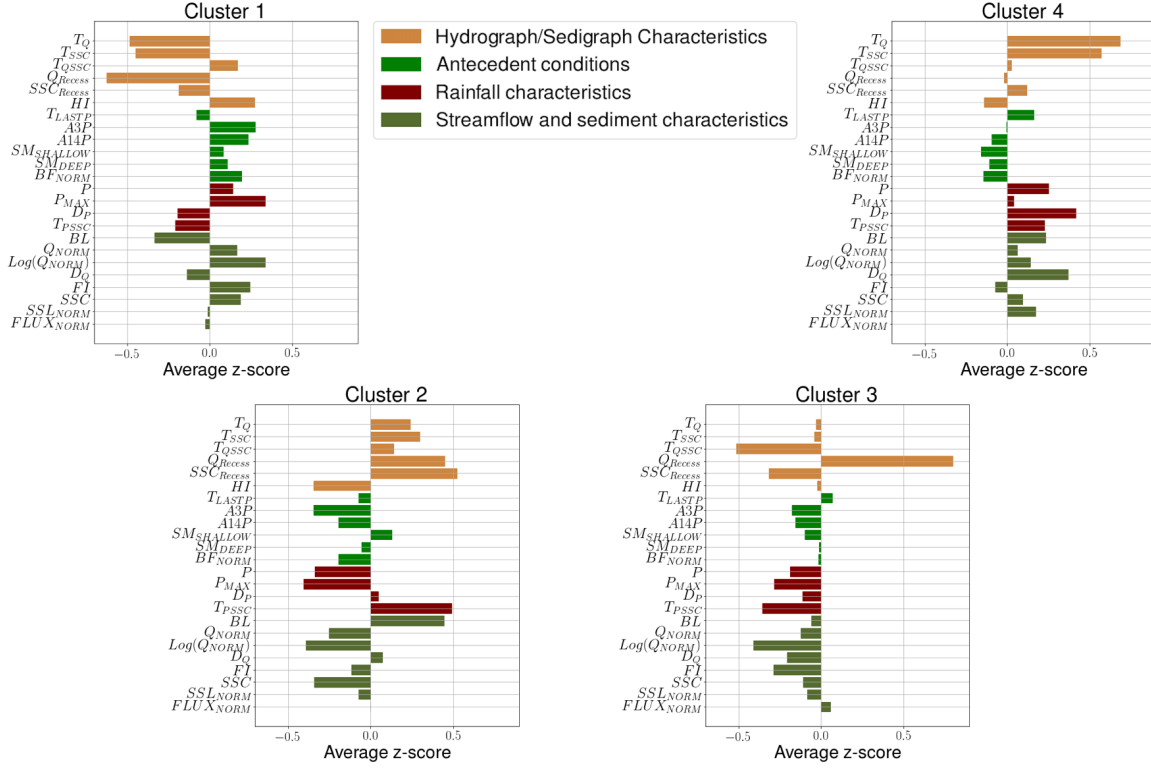


Figure 15: Average z-scores of storm event metrics for each of the four clusters.

Each of the four clusters exhibited certain characteristics of events, observed from the event visualizations (see Figure 12) and the z-score value of storm event metrics (see Figure 15). The metrics were used not as input to the clustering algorithm but as means to study the characteristics of resulting clusters.

Storm events in the cluster 1 were larger events with wetter antecedent conditions that result in higher streamflows and higher SSC. These characteristics are based on the following observations. First, the events have larger amount of precipitation (positive z-score for P and P_{MAX}) resulting in larger streamflows (positive z-score for $Log(Q_{NORM})$, Q_{NORM} , and FI). Second, the events have positive z-score for BF_{NORM} , SM_{DEEP} , $SM_{SHALLOW}$, $A3P$ and $A14P$, which characterize wetter antecedent conditions. Other key characteristics are that their hydrographs do not return quickly to baseline flow, sedigraph pulses occur early, and the dominating hysteresis shape is a broad clockwise pattern (see Figure 12a). The hysteresis pattern is also confirmed from positive z-score of HI . Additional event characteristics include negative z-score of T_{SSC} and T_Q , meaning quickly rising sedigraph and hydrograph, respectively, and negative z-score of Q_{Recess} and SSC_{Recess} , meaning that streamflow and SSC, respectively, return to base levels at the end of the events.

Cluster 2 included smaller storm events with drier antecedent conditions in which the streamflow and SSC do not return to base levels at the end of the events. These characteristics are based on the following observations. First, the events have smaller amount of precipitation (negative z-score of P and P_{MAX}), resulting in smaller streamflows (negative z-score of $Log(Q_{NORM})$, Q_{NORM} , and FI). Second, the events have negative z-score values for BF_{NORM} , SM_{DEEP} , $SM_{SHALLOW}$, $A3P$ and $A14P$, which characterize drier antecedent conditions. Third, the events have positive z-score values for Q_{Recess} and SSC_{Recess} , meaning that the streamflow and the SSC do not return to base levels at the end of the events (see Figure 12b). Other

key characteristics include a longer time from peak SSC to peak rainfall center of mass (positive z-score of T_{PSSC}) and that the dominating hysteresis shape is a narrow loop (see Figure 12b). The hysteresis pattern is also confirmed from negative z-score of hysteresis index. Additional characteristics include a negative z-score of SSC , meaning a lower peak SSC amount, and a negative z-score of BL , meaning that the watersheds respond slowly to a rainfall event.

Cluster 3 included smaller events that occurred in average antecedent conditions in which streamflow does not completely return to baseflow and SSC also lingers above base-level or is multi-peaked. These characteristics are based on the following observations. First, the events have smaller amount of precipitation (negative z-score of P and P_{Max}), resulting in smaller streamflows (negative z-score of $\text{Log}(Q_{Norm})$, Q_{Norm} , and FI). Second, the events have near zero z-score values for BF_{Norm} , SM_{Deep} , $SM_{Shallow}$, $A3P$ and $A14P$, which characterize average antecedent conditions. Third, the events have a positive z-score for Q_{Recess} and negative z-score for SSC_{Recess} , meaning that the streamflow does not completely return to baseflow while SSC does. It can be observed from Figure 12c that SSC lingers or is multi-peaked. Other key characteristics include a short time from peak SSC to peak rainfall center of mass (negative z-score of T_{PSSC}) and short time from peak discharge to peak SSC (negative z-score of T_{QSSC}). Additional characteristics include a fast rate of rise for both streamflow and SSC (see Figure 12c).

Cluster 4 included longer and less intense events occurring during average to slightly dry antecedent conditions. These characteristics are based on the following observations. First, the events have longer duration (positive z-score of D_Q) and high total precipitation (positive z-score of P) but low maximum precipitation (negative z-score of P_{Max}) resulting in near average streamflows (near zero z-score for $\text{Log}(Q_{Norm})$, Q_{Norm} , and FI). Second, the events have slightly negative z-score values for BF_{Norm} , SM_{Deep} , $SM_{Shallow}$, $A3P$ and $A14P$, which characterize average to slightly dry antecedent conditions. Other key characteristics include long time to peak SSC and Q (positive z-score for T_{SSC} and T_Q). Additional characteristics include a larger amount of sediments transported during an event (positive SSL_{Norm}).

5 Discussion

5.1 Hydrological implications of the results

Main implications we can draw from the results are that in the Mad River watershed (i) the optimal number of categories of storm events is four (see Figure 11); (ii) events in computational clusters have significant relationships to events in hysteresis loop classes and events in watershed sites, while not identical (see Figure 13 and Figure 14); (iii) metrics that differentiate events in computational clusters are different from metrics that differentiate events in hysteresis loop classes (see Table 7); (iv) events in different computational clusters are significantly different in terms of metrics associated with hydrograph and sedigraph characteristics (see Table 7); and (v) events in each cluster share certain unique characteristics in terms of all 24 storm event metrics (see Figure 15).

The results also suggest that the computational clustering approach identified events caused by sediment delivery from upstream sources. Hysteresis approach is typically used only for small sized watersheds (smaller than 100 km^2) since large watershed are affected by sediment delivery from upstream sources (Hamshaw et al., 2018). In our results, however, the cluster 2 is dominated by events from the main stem of Mad River watershed, while events in the cluster 2 have smaller precipitations and stream flow and sediment flow do not come back to the base level. These are indicative of consistent sediment and streamflow delivery from upstream sources that might be experiencing or might have experienced a storm event shortly before. Additionally, streamflow not returning to the base level at the end of an event is likely to indicate saturated soils, high groundwater tables or soil moisture, a feature that the current classification schemes based on hysteresis shape/direction cannot capture. Since the computational clustering captured this difference in

discharge values at the start and end of the event, it could be a promising addition to methods used to create an early warning system for impending floods.

5.2 Challenges and opportunities

The sparsity of data is an inherent challenges in storm event analysis. Our study area — a typical humid and temperate watershed — experiences only about 30 storm events a year. Other recent prominent event-based studies (Wymore et al., 2019; Sherriff et al., 2016; Vaughan et al., 2017) featured between 8 and 90 events per site monitored. This inherent sparsity of data is compounded when analyzing multivariate time series generated from sensors, as all sensors of different modality must be online and operational simultaneously, which is a significant challenge in *in-situ* water quality monitoring. Besides, increased dimensionality (i.e., number of variables) of data would cause storm events to be even sparser (called the “curse of dimensionality” (Bellman, 1957)). Currently, efforts are being made in the field of hydrology to compile larger datasets across researchers and organizations (CUAHSI, 2019) to address the data sparsity issue. Generating synthetic storm events as was done in our work could be another approach.

Determining the optimal value of k , the number of clusters of storm events, is challenging in a hydrological application like ours where there is not always clear separation of groups. Using the elbow method can be subjective, and sometimes the characteristic elbow is not clearly visible in an elbow plot. If identifying the elbow becomes problematic, we may consider different options for the analysis steps such as preprocessing, distance measure, and clustering algorithm. Regarding the clustering algorithm for example, a density-based clustering algorithm (Ester et al., 1996), which does not require the number of clusters as an input, can be considered.

The computational clustering approach used in this work is also applicable to other solutes (or constituents) that demonstrate patterns different from those that are observed in SSC (Lloyd et al., 2016a; Zuecco et al., 2016). Moreover, the computational approach can be extended beyond using a single solute (e.g., SSC) to using multiple solutes (e.g., SSC, phosphorous, CO₂) together in order to reveal any unknown interactions among them in watershed events.

References

- Aguilera, R. and Melack, J. M. (2018). Concentration-discharge responses to storm events in coastal california watersheds. *Water Resources Research*, 54(1):407424.
- Banerjee, A. and Dave, R. N. (2004). Validating clusters using the hopkins statistic. In *Proceedings of the 2004 IEEE International Conference on Fuzzy Systems (IEEE Cat. No.04CH37542)*, volume 1, pages 149–153 vol.1.
- Begum, N., Ulanova, L., Wang, J., and Keogh, E. (2015). Accelerating dynamic time warping clustering with a novel admissible pruning strategy. In *Proceedings of the 21th ACM SIGKDD International Conference on Knowledge Discovery and Data Mining, KDD ’15*, pages 49–58, New York, NY, USA. ACM.
- Bellman, R. (1957). *Dynamic Programming*. Dover Publications.
- Bende-Michl, U., Verburg, K., and Cresswell, H. P. (2013). High-frequency nutrient monitoring to infer seasonal patterns in catchment source availability, mobilisation and delivery. *Environmental Monitoring and Assessment*, 185(11):9191–9219.

- Burns, D. A., Pellerin, B. A., Miller, M. P., Capel, P. D., Tesoriero, A. J., and Duncan, J. M. (2019). Monitoring the riverine pulse: Applying high-frequency nitrate data to advance integrative understanding of biogeochemical and hydrological processes. *Wiley Interdisciplinary Reviews: Water*, page e1348.
- Burt, T. P., Worrall, F., Howden, N. J. K., and Anderson, M. G. (2015). Shifts in discharge-concentration relationships as a small catchment recover from severe drought. *Hydrological Processes*, 29(4):498507.
- Chen, L., Sun, C., Wang, G., Xie, H., and Shen, Z. (2017). Event-based nonpoint source pollution prediction in a scarce data catchment. *Journal of Hydrology*, 552(Supplement C):1327.
- CUAHSI (2019). Consortium of universities for the advancement of hydrologic science, inc. <https://www.cuahsi.org>.
- Dau, H. A., Keogh, E., Kamgar, K., Yeh, C.-C. M., Zhu, Y., Gharghabi, S., Ratanamahatana, C. A., Yanping, Hu, B., Begum, N., Bagnall, A., Mueen, A., and Batista, G. (2018). The UCR time series classification archive. https://www.cs.ucr.edu/~eamonn/time_series_data_2018/.
- Ehret, U. and Zehe, E. (2011). Series distance - an intuitive metric to quantify hydrograph similarity in terms of occurrence, amplitude and timing of hydrological events. *Hydrology and Earth System Sciences*, 15(3):877–896.
- Ester, M., Kriegel, H.-P., Sander, J., and Xu, X. (1996). A density-based algorithm for discovering clusters a density-based algorithm for discovering clusters in large spatial databases with noise. In *Proceedings of the Second International Conference on Knowledge Discovery and Data Mining*, KDD’96, pages 226–231. AAAI Press.
- Ewen, J. (2011). Hydrograph matching method for measuring model performance. *Journal of Hydrology*, 408(1):178 – 187.
- Hamshaw, S., M. Dewoolkar, M., W. Schroth, A., Wemple, B., and M. Rizzo, D. (2018). A new machine-learning approach for classifying hysteresis in suspended-sediment discharge relationships using high-frequency monitoring data. *Water Resources Research*, 54.
- Javed, A. (2019a). Dynamic time warping. <https://github.com/ali-javed/dynamic-time-warping>.
- Javed, A. (2019b). Multivariate time series dynamic time warping using euclidean distance. <https://github.com/ali-javed/Multivariate-Kmedoids>.
- Jones, A. S., Stevens, D. K., Horsburgh, J. S., and Mesner, N. O. (2011). Surrogate measures for providing high frequency estimates of total suspended solids and total phosphorus concentrations1. *JAWRA Journal of the American Water Resources Association*, 47(2):239–253.
- Keesstra, S. D., Davis, J., Masselink, R. H., Casal, J., Peeters, E. T. H. M., and Dijkma, R. (2019). Coupling hysteresis analysis with sediment and hydrological connectivity in three agricultural catchments in navarre, spain. *Journal of Soils and Sediments*, 19(3):15981612.
- Latecki, L. J., Megalooikonomou, V., Qiang Wang, Lakaemper, R., Ratanamahatana, C. A., and Keogh, E. (2005). Partial elastic matching of time series. In *Proceedings of the 5th IEEE International Conference on Data Mining (ICDM’05)*, pages 4 pp.–.
- Latecki, L. J., Megalooikonomou, V., Wang, Q., Lakaemper, R., Ratanamahatana, C. A., and Keogh, E. (2005). Elastic partial matching of time series. In Jorge, A. M., Torgo, L., Brazdil, P., Camacho, R., and Gama, J., editors, *Knowledge Discovery in Databases: PKDD 2005*, pages 577–584, Berlin, Heidelberg. Springer Berlin Heidelberg.

- Lloyd, C., Freer, J., Johnes, P., and Collins, A. (2016a). Using hysteresis analysis of high-resolution water quality monitoring data, including uncertainty, to infer controls on nutrient and sediment transfer in catchments. *Science of The Total Environment*, 543, Part A:388 – 404.
- Lloyd, C. E. M., Freer, J. E., Johnes, P. J., and Collins, A. L. (2016b). Technical note: Testing an improved index for analysing storm discharge–concentration hysteresis. *Hydrology and Earth System Sciences*, 20(2):625–632.
- Mather, A. L. and Johnson, R. L. (2015). Event-based prediction of stream turbidity using a combined cluster analysis and classification tree approach. *Journal of Hydrology*, 530:751 – 761.
- Minaudo, C., Dupas, R., Gascuel-Oudou, C., Fovet, O., Mellander, P.-E., Jordan, P., Shore, M., and Moatar, F. (2017). Nonlinear empirical modeling to estimate phosphorus exports using continuous records of turbidity and discharge. *Water Resources Research*, 53.
- Onderka, M., Krein, A., Wrede, S., Martinez-Carreras, N., and Hoffmann, L. (2012). Dynamics of storm-driven suspended sediments in a headwater catchment described by multivariable modeling. *Journal of Soils and Sediments*, 12(4):620–635.
- Paparrizos, J. and Gravano, L. (2016). K-shape: Efficient and accurate clustering of time series. *SIGMOD Record*, 45(1):69–76.
- Paparrizos, J. and Gravano, L. (2017). Fast and accurate time-series clustering. *ACM Transactions on Database Systems*, 42(2):8:1–8:49.
- PRISM (2019). PRISM climate group. <http://prism.oregonstate.edu>. Last accessed on March 16, 2019.
- Rakthanmanon, T., Campana, B., Mueen, A., Batista, G., Westover, B., Zhu, Q., Zakaria, J., and Keogh, E. (2012). Searching and mining trillions of time series subsequences under dynamic time warping. In *Proceedings of the 18th ACM SIGKDD International Conference on Knowledge Discovery and Data Mining*, pages 262–270.
- Ratanamahatana, C. A. and Keogh, E. (2004). Everything you know about dynamic time warping is wrong. In *Proceedings of the 3rd Workshop on Mining Temporal and Sequential Data*. Citeseer.
- Rose, L. A., Karwan, D. L., and Godsey, S. E. (2018). Concentration-discharge relationships describe solute and sediment mobilization, reaction, and transport at event and longer timescales. *Hydrological Processes*, 32(18):2829–2844.
- Rosenberg, A. and Hirschberg, J. (2007). V-measure: A conditional entropy-based external cluster evaluation measure. In *Proceedings of the 2007 Joint Conference on Empirical Methods in Natural Language Processing and Computational Natural Language Learning*, pages 410–420.
- Sakoe, H. and Chiba, S. (1978). Dynamic programming algorithm optimization for spoken word recognition. *IEEE Transactions on Acoustics, Speech, and Signal Processing*, 26(1):43–49.
- Satopaa, V., Albrecht, J., Irwin, D., and Raghavan, B. (2011). Finding a “kneedle” in a haystack: Detecting knee points in system behavior. In *Proceedings of the 31st International Conference on Distributed Computing Systems Workshops*, pages 166–171.
- Scipy (2012). Savitzky golay filtering. <https://scipy-cookbook.readthedocs.io/items/SavitzkyGolay.html>. Last accessed on February 13, 2019.

- Scipy (2019). Savitzky golay filtering. <https://docs.scipy.org/doc/scipy/reference/generated/scipy.interpolate.UnivariateSpline.html>. Last accessed on February 13, 2019.
- Sherriff, S. C., Rowan, J. S., Fenton, O., Jordan, P., Melland, A. R., Mellander, P.-E., and hUallachain, D. O. (2016). Storm event suspended sediment-discharge hysteresis and controls in agricultural watersheds: Implications for watershed scale sediment management. *Environmental Science & Technology*, 50(4):17691778.
- Shokoohi-Yekta, M. and Keogh, E. J. (2015). On the non-trivial generalization of dynamic time warping to the multi-dimensional case. In *Proceedings of the 2015 SIAM International Conference on Data Mining*.
- Stryker, J., Wemple, B., and Bomblies, A. (2017). Modeling sediment mobilization using a distributed hydrological model coupled with a bank stability model. *Water Resources Research*, 53(3):2051–2073.
- Vaughan, M. C. H., Bowden, W. B., Shanley, J. B., Vermilyea, A., Sleeper, R., Gold, A. J., Pradhanang, S. M., Inamdar, S. P., Levia, D. F., Andres, A. S., and et al. (2017). High-frequency dissolved organic carbon and nitrate measurements reveal differences in storm hysteresis and loading in relation to land cover and seasonality: high-resolution doc and nitrate dynamics. *Water Resources Research*, 53(7).
- Wemple, B. C., Clark, G. E., Ross, D. S., and Rizzo, D. M. (2017). Identifying the spatial pattern and importance of hydro-geomorphic drainage impairments on unpaved roads in the northeastern usa. *Earth Surface Processes and Landforms*, 42(11):1652–1665.
- Wendi, D., Merz, B., and Marwan, N. (2019). Assessing hydrograph similarity and rare runoff dynamics by cross recurrence plots. *Water Resources Research*, 55(6):4704–4726.
- Wikipedia (2019). Synthetic data. https://en.wikipedia.org/wiki/Synthetic_data.
- Williams, G. P. (1989). Sediment concentration versus water discharge during single hydrologic events in rivers. *Journal of Hydrology*, 111(1):89 – 106.
- Williams, M. R., Livingston, S. J., Penn, C. J., Smith, D. R., King, K. W., and Huang, C.-h. (2018). Controls of event-based nutrient transport within nested headwater agricultural watersheds of the western lake erie basin. *Journal of Hydrology*, 559:749761.
- Wu, X., Kumar, V., Ross Quinlan, J., Ghosh, J., Yang, Q., Motoda, H., McLachlan, G. J., Ng, A., Liu, B., Yu, P. S., Zhou, Z.-H., Steinbach, M., Hand, D. J., and Steinberg, D. (2007). Top 10 algorithms in data mining. *Knowledge and Information Systems*, 14(1):1–37.
- Wymore, A. S., Leon, M. C., Shanley, J. B., and McDowell, W. H. (2019). Hysteretic response of solutes and turbidity at the event scale across forested tropical montane watersheds. *Frontiers in Earth Science*, 7:126.
- Zuecco, G., Penna, D., Borga, M., and van Meerveld, H. J. (2016). A versatile index to characterize hysteresis between hydrological variables at the runoff event timescale. *Hydrological Processes*, 30(9):1449–1466.